

## Joule heating in single-walled carbon nanotubes

Tarek Ragab and Cemal Basaran<sup>a)</sup>

*Electronic Packaging Laboratory, State University of New York at Buffalo, New York 14260-4300, USA*

(Received 26 March 2009; accepted 20 July 2009; published online 18 September 2009)

Joule heating in single-walled carbon nanotubes (CNTs) using a quantum mechanical approach is presented in this paper. The modeling is based on the energy transfer between the electrons and both acoustic and optical phonons. In this formulation, only the knowledge of the full energy dispersion relation, phonon dispersion relation, and the electron-phonon coupling potential is required for the calculations. For verification of the proposed model, the current-voltage relation for extremely long nanotubes is calculated and the results are compared with the experimental data. The electric field dependence of the amount of energy generated by Joule heating is plotted. Moreover the effect of the thermal environment on the behavior of Joule heating is studied. The formulation proposed in this paper can also be used for structures other than CNTs. Computations indicate that, contrary to popular opinion, metallic CNT does not follow Joule's law of  $P=IV$ . Joule heating in CNT is significantly less than what is predicted with Joule law ( $P=IV$ ), which would make it a perfect candidate to replace copper as interconnect material in electronics. © 2009 American Institute of Physics. [doi:10.1063/1.3204971]

### I. INTRODUCTION

Carbon nanotubes (CNTs) are the single atom thick tubes formed by wrapping a sheet of graphite made out of hexagonally arranged carbon atoms. The direction of folding this graphite sheet is defined by the chiral vector  $C_h(n,m)$ ,<sup>1</sup> where CNTs can be classified into chiral nanotubes  $(n,m)$ , zigzag nanotubes  $(n,0)$ , and armchair nanotubes  $(n,n)$ .

CNTs are one of the most studied materials in the past decade due to their promising mechanical,<sup>2</sup> electrical, and thermal<sup>3</sup> properties. The effect of the temperature generated due to Joule heating on the electrical transport properties of metallic single-walled CNTs (SWCNTs) has been investigated in some recent studies.<sup>3-7</sup> In these studies Joule heating is identified to be dependent on the macroscopic "bulk" resistance of the CNT under investigation without any consideration for the underlying quantum mechanics of the Joule heating.

Horsfield and co-workers<sup>8-12</sup> studied the Joule heating in nanoscale devices using classical, semiclassical, and quantum mechanical formulations by coupling the electronic and atomic dynamics. This modeling technique is called the correlated electron-ion dynamics (CEID). In CEID the power delivered to the atoms consists of a heating term and a cooling term.

In this paper, similar to the CEID model, the electrons are excited by the electrical current, and then the Joule heating is identified from the response of the ionic motion to this excitation of the electrons. A quantum mechanical formulation of the Joule heating in SWCNTs is derived based on the energy transfer to the ionic motion in response to the excitation of the electrons under electrical current. The only connection between the formulation used in this paper and the CEID model is the concept that the Joule heating can be calculated from the ionic response to the electrical current

without any further relations. Our formulation starts from the basic concepts of quantum mechanics to write a formula for the Joule heating. As a case study, the effect of the temperature and the electric field on the power generated in a (10,10) single-walled armchair CNT is studied.

### II. QUANTUM PHYSICS OF JOULE HEATING

Joule heating is the heat generated in a metal conductor due to the flow of electricity within it and losing part of its energy to the vibration of the lattice (phonons). Electrons migrating through the device under the effect of an electrical field undergo different scattering events, namely, scattering with phonons, ionized impurities, and vacancies as well as electron-electron scattering. Due to the large mass of the impurities in comparison with the mass of the electron, scattering with impurities is completely elastic and does not involve a transfer of energy from the electron to the lattice.<sup>13</sup> Also the electron-electron scattering does not have any effect on the temperature of the lattice, and thus the only scattering mechanism that plays a role in heating the lattice is the electron-phonon scattering mechanisms and these are the only mechanisms considered in this study.

In this formulation, we calculate the Joule heating power as the energy transferred to the lattice from electron scattering between different states multiplied by the rate by which these scattering can occur. This should be integrated over all the electron states to yield the total Joule heating power.

For an electron initially in state  $\mathbf{k}$  having an energy  $E(\mathbf{k})$  and scattering to a final state  $\mathbf{k}'$  with energy  $E(\mathbf{k}')$ , the energy transferred to or from the lattice in this event will be  $E(\mathbf{k}') - E(\mathbf{k})$ , which can be positive, representing cooling the lattice, or negative, representing heating the lattice. For this scattering to happen, there must be a phonon state of momentum  $\hbar\mathbf{q} = \hbar(\mathbf{k}' - \mathbf{k})$  and energy  $E(\mathbf{q}) = E(\mathbf{k}') - E(\mathbf{k})$  in order for the momentum and the energy to be conserved. In this paper electrons scattering to states in the second Brillouin zone are considered.

<sup>a)</sup>Electronic mail: cjb@buffalo.edu.

loun zone (Umklapp processes) are included as well as scattering to states in the first Brillouin zone (normal processes). For this scattering event the power transferred to or from the lattice would be  $[E(\mathbf{k}') - E(\mathbf{k})]S_m(\mathbf{k}, \mathbf{k}')$ , where  $S_m(\mathbf{k}, \mathbf{k}')$  is the number of scatterings per unit time (scattering rate) for an electron in state  $\mathbf{k}$  scattering to state  $\mathbf{k}'$  due to the scattering mechanism  $m$ . For electron-phonon scattering, the probability  $S_m(\mathbf{k}, \mathbf{k}')$  can be calculated using the first order perturbation theory from Fermi's golden rule as<sup>13</sup>

$$S_m(\mathbf{k}, \mathbf{k}') = \frac{2\pi}{\hbar} |\langle \psi_{\mathbf{k}'} | \hat{H}^{\text{ep}} | \psi_{\mathbf{k}} \rangle|^2 \delta[E(\mathbf{k}') - E(\mathbf{k}) \pm \hbar\omega], \quad (1)$$

where  $|\psi_{\mathbf{k}}\rangle$  and  $|\psi_{\mathbf{k}'}\rangle$  are the initial and final states, respectively,  $\pm \hbar\omega$  is the phonon energy emitted or absorbed, and  $\hat{H}^{\text{ep}}$  is the electron-phonon interaction operator. Thus, in this formulation the electron-phonon interaction is implicitly included through the scattering probability term and is temperature-dependent through the Bose-Einstein occupation number. Taking into account the probability that the electron occupies the state  $\mathbf{k}$  and that state  $\mathbf{k}'$  is empty and integrating over all the states in the first Brillouin zone and summing over all the allowed scattering mechanisms, we get the total power per unit volume as

$$w = \left( \frac{1}{4\pi^3} \right)^2 \sum_m \int \int [E(\mathbf{k}') - E(\mathbf{k})] S_m(\mathbf{k}, \mathbf{k}') f(\mathbf{k}) [1 - f(\mathbf{k}')] d\mathbf{k}' d\mathbf{k}, \quad (2)$$

where  $f(\mathbf{k})$  is the Fermi-Dirac distribution function in the presence of an electric field  $\mathbf{E}$ . Using the relaxation time approximation ( $\partial f(\mathbf{k}) / \partial t = -\{[f(\mathbf{k}) - f^0(\mathbf{k})] / \tau\}$ ) along with Taylor's expansion and neglecting second order terms and higher in the expansion,  $f(\mathbf{k})$  can be given as<sup>14</sup>

$$f(\mathbf{k}) = f^0[E(\mathbf{k}) - e\tau(\mathbf{k})\mathbf{v}_{\mathbf{k}} \cdot \mathbf{E}], \quad (3)$$

where  $f^0[E(\mathbf{k})]$  is Fermi-Dirac distribution function,  $\mathbf{v}_{\mathbf{k}}$  is the group velocity vector of wave packet centered about the state  $\mathbf{k}$ , and  $\tau(\mathbf{k})$  is the relaxation time, which for isotropic scattering (which is the case for electron-phonon scattering in SWCNTs) is calculated as the summation over all available final states for all the allowable scattering mechanisms and is written as<sup>13</sup>

$$\tau(\mathbf{k}) = \frac{1}{\sum_m \sum_{\mathbf{k}'} S_m(\mathbf{k}, \mathbf{k}')}. \quad (4)$$

According to Ref. 13, this value for  $\tau(\mathbf{k})$  is valid when  $|\mathbf{v}_{\mathbf{k}}|$  is constant, which is the case for metallic CNTs near the Fermi surface.

In the formulation given above, the scattering probability and the energy dispersion relation are the only required information in order to calculate the Joule heating power. The scattering probabilities can be calculated from Fermi's golden rule based on the knowledge of the electron and phonon dispersion relations as well as the atomic configuration of the lattice of the material under consideration.

In this paper an equilibrium Bose-Einstein distribution is used for predicting the phonon population, which is used in calculating the scattering rates as shown in the next sec-

tion. For future research, we are working on improving the model to include the hot phonon effect to predict the temporal evolution of the Joule heating against the snapshot behavior predicted in this paper. To include the hot phonon effect, phonon-phonon scattering as well as the thermal coupling between the nanotube and the substrate should be available. Calculations on predicting the thermal coupling as well as the phonon population in SWCNTs were published recently this year.<sup>15</sup>

### III. APPLICATION TO (10,10) CNT

In this section the formulation developed above is used to compute the Joule heating in a (10,10) metallic armchair CNT with diameter ( $d$ ) of 13.6 Å. Here we consider scattering with longitudinal acoustic (LA) and longitudinal optical (LO) phonons only. This is because the transverse out-of-plane and in-plane modes would have very low scattering probabilities in comparison with the longitudinal modes.<sup>16-19</sup> The scattering mechanisms considered here are phonon absorption and emission as well as forward and backward scatterings, thus having a total of eight scattering mechanisms.

Since a CNT is formed by folding the two-dimensional graphite sheet into a cylinder along the chiral vector direction  $C_h$ , the wavevector  $\mathbf{k}(k_x, k_y)$  is represented better as  $\mathbf{k}(k_{\perp}, k_{\parallel})$ , where  $k_{\parallel}$  and  $k_{\perp}$  are the reciprocal lattice vectors along the nanotube axis and circumferential directions, respectively.<sup>20</sup> Due to the periodicity of the lattice along the circumference, the wavevector is quantized along the direction of  $k_{\perp}$  having a quantum number  $\nu$  but considered continuous in the direction of  $k_{\parallel}$  having any value  $k$  for long CNTs, resulting in a series of one-dimensional subbands. This is known as the zone folding method.<sup>20</sup> For phonons, variables  $(q, \mu)$  are used to define the wavevector and quantum number of the subband instead of  $(k, \nu)$  to differentiate between phonon and energy states. For the (10,10) CNT under consideration, there are 20 different subbands, 11 of which are distinct subbands and nine of which are doubly degenerate.

The energy dispersion relation for a graphite sheet was calculated using the tight binding method for graphite, and the phonon dispersion relation was calculated based on a fourth-nearest-neighbor force constant model with parameters that fit the experimental data.<sup>20</sup> The energy and the phonon dispersion relations were then generated from that of graphene using the zone folding method, where the full band was considered in the calculations. Figure 1 shows the energy dispersion relation for the  $\pi^*$  antibonding energies, while Fig. 2 shows the phonon dispersion relation for both LA and LO phonons.

The scattering probability due to LA and LO phonons are calculated from Eq. (1) using the first order perturbation theory and the deformation-potential approximation according to the following two equations, respectively:<sup>19,21-23</sup>

$$S[(k, \nu), (k', \nu')] = \frac{\hbar D_{\text{LA}}^2 [q^2 + (2\mu/d)^2]}{2\rho E_p^{\text{LA}}(q, \mu)} \left\{ N[E_p^{\text{LA}}(q, \mu)] + \frac{1}{2} \pm \frac{1}{2} \right\} \left| \frac{dE}{dk} \right|_{(k', \nu')}^{-1}, \quad (5)$$

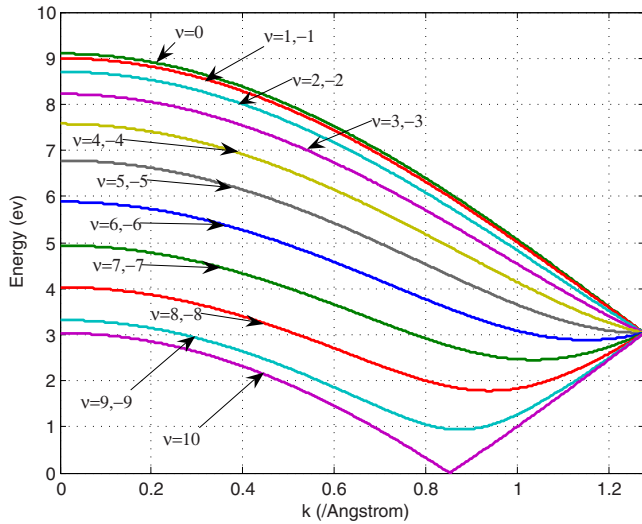


FIG. 1. (Color online) Energy dispersion for (10,10) CNT along the positive part of the wavevector for the  $\pi^*$  antibonding energies.

$$S[(k, \nu), (k', \nu')] = \frac{\hbar D_{LO}^2}{2\rho E_p^{LO}(q, \mu)} \left\{ N[E_p^{LO}(q, \mu)] + \frac{1}{2} \pm \frac{1}{2} \right\} \times \left| \frac{dE}{dk} \right|_{(k', \nu')}^{-1}, \quad (6)$$

where  $D_{LA}$  and  $D_{LO}$  are the deformation-potential constants for the LA and LO phonons, respectively,  $\hbar$  is the modified Planck's constant,  $\rho$  is the linear mass density of the CNT,  $|dE/dk|^{-1}$  is the density of state,  $N[E_p(q, \mu)]$  is the Bose-Einstein occupation number for a phonon in the state  $(q, \mu)$ , and the positive and negative signs indicate emitting or absorbing a phonon, respectively. Here, electrons only scatter if the energy is conserved  $[E(k, \nu) - E(k', \nu') = \pm E_p(q, \mu)]$  as well as the momentum along the tube axis and the circumferential directions ( $k - k' = \pm q$  and  $\nu - \nu' = \pm \mu$ ). That means that for every electron state  $(k, \nu)$  interacting with a phonon subband  $\mu$ , there can be only one final state for each of the eight scattering mechanisms mentioned above, which gives us a maximum number of 160 final states for every state

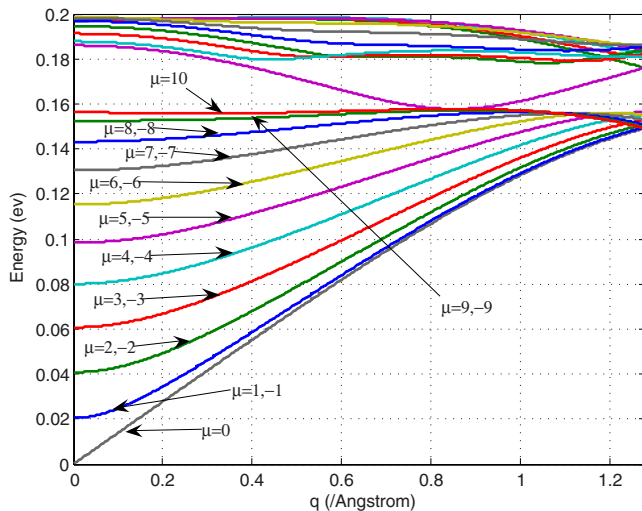


FIG. 2. (Color online) Phonon dispersion relation for (10,10) CNT. The lower energy is LA phonons, and the upper energy is LO phonons.

$(k, \nu)$ . The computed total scattering rates for the lowest two subbands ( $\nu=10, \nu=\pm 9$ ) are plotted in Fig. 3; this calculation agrees very well with that obtained by fitting experimental data,<sup>24</sup> which have average values of the order of  $10^{13}$  and  $10^{14} \text{ s}^{-1}$  for acoustic and optical phonon backscatterings, respectively.

Because there are only 160 discrete possible final states, the integral in Eq. (2) can be converted to summation over these states. Hence, we can rewrite Eq. (2) for the specific (10,10) CNT to get the Joule heating power per unit length as

$$w = \frac{1}{\pi} \sum_{m=1}^{160} \sum_{\nu=-9}^{10} \int [E(k', \nu')_m - E(k, \nu)] S_m[(k, \nu), (k', \nu')_m] f(k, \nu) \times \{1 - f[(k', \nu')_m]\} dk. \quad (7)$$

#### IV. RESULTS AND DISCUSSION

In order to validate the calculations presented above, the current-voltage relationship for a (10,10) CNT is calculated using a model that has the merit of our proposed model for calculating the Joule heating. Here, the electric current through a (10,10) CNT is given by<sup>14</sup>

$$I = \frac{e}{\pi} \sum_{\nu=-9}^{10} \int f(k, \nu) \frac{1}{\hbar} \frac{\partial E}{\partial k} dk. \quad (8)$$

The intensity of the current is calculated at different electric field forces, and results are plotted against the experimental measurements of Park *et al.*<sup>25</sup> in Fig. 4. The lower saturation current value measured from the experiments can be attributed to the scattering with impurities or defects along the length of the CNT, which is the reason for higher saturation current in shorter CNT.<sup>24,25</sup> We should also point out that the chirality and defect and impurity state of the tested CNT are unknown.<sup>25</sup> Moreover the experimental data represent resistance of the composite system of CNT and gold pads, not the CNT alone. It is also clear from the experimental results<sup>25</sup> that as the length of the nanotubes increases, the slope of the curve becomes steeper, and thus we would expect that for the limit of an infinite CNT, the initial slope would tend to that calculated from Eq. (8). The slope of the curve at higher electric fields can be realized from the fact that curves calculated from Eq. (8) were calculated at constant temperatures, but as time evolves the temperature will change due to Joule heating and thus the slope will decrease (Fig. 5). This was also proposed and proven theoretically by Kuroda and Leburton.<sup>7</sup>

Figure 6 presents the Joule heating power per unit length of the (10,10) CNT calculated from the model derived in Eq. (7), and it is plotted against classical power law ( $P=IV$ ) [Eq. (8)] and also against values computed from  $I-V$  experimental data.<sup>25</sup> It should be pointed out that  $P=IV$  calculated from experimental data is not measured Joule heating data. It is clear from Fig. 6 that the quantum mechanical model gives Joule heating power that is two orders of magnitude less than what is predicted by  $P=IV$ . This finding is also supported by measurements reported by Deshpande *et al.*,<sup>26</sup> authors ex-

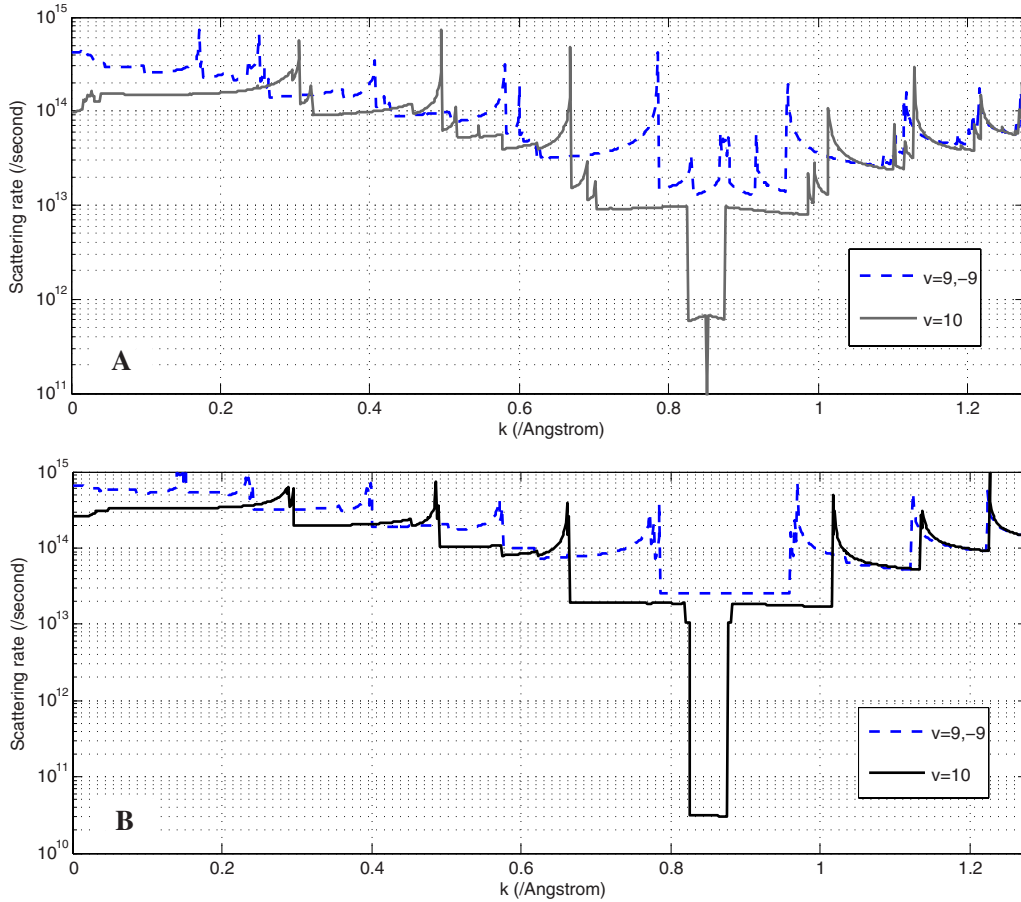


FIG. 3. (Color online) The scattering rates for LA phonons (a) and LO phonons (b) for the lowest two subbands at room temperature.

licitly state that “the lattice cannot dissipate  $6 \mu\text{W}$  of power without heating to extremely high temperatures. However, such lattice heating is not supported by our observation.” This is because in the quantum mechanical model, only scattering events that involve energy transfer are considered to contribute to the Joule heating, while the rest of the scattering events that would contribute to the resistance but would not contribute to the Joule heating is not considered. These scattering events include electron-phonon scattering that only involves momentum transfer, which is considered in this study, as well as scatterings with impurities

and defects that are not included in this study. Thus omitting the electron scattering with impurities and defects would only affect the  $I$ - $V$  characteristics [Eq. (8)] of the CNT but should have no effect on the Joule heating power generated [Eq. (7)]. Also in Fig. 6, the amount of Joule heating power generated seems to come to a constant value at an electric field of around 2 KV/cm, after which increasing the electric field has no significant effect on the amount of power generated. This can be explained by the fact that after that upper

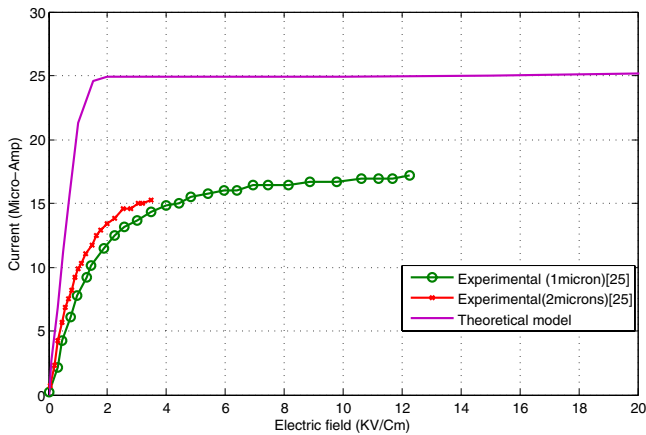


FIG. 4. (Color online) Experimental data vs theoretical  $I$ - $V$  curves for metallic SWCNTs at 300 K.

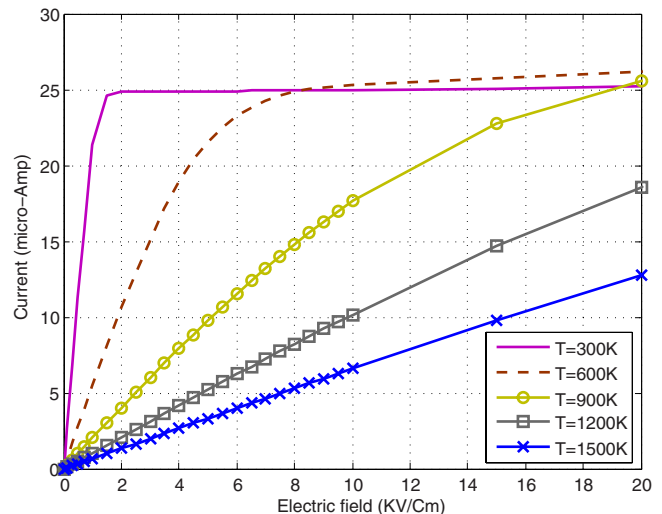


FIG. 5. (Color online) Theoretical  $I$ - $V$  curves at different temperatures.

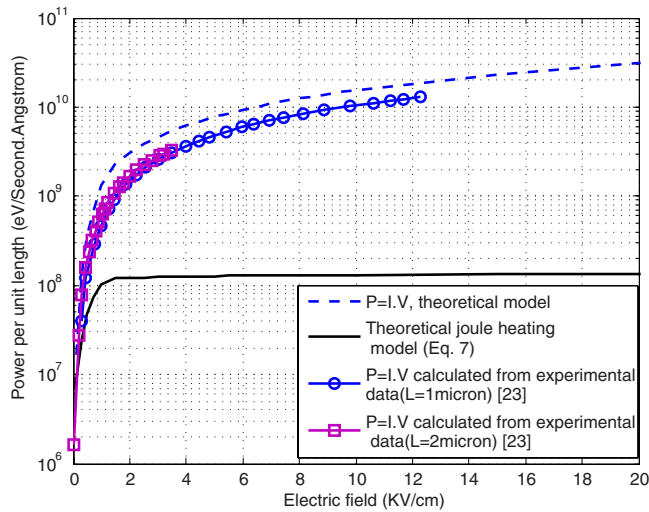


FIG. 6. (Color online) Comparison of theoretical and experimental data of Joule heating in CNT at 300 K.

limit electric field force, the lowest energy subband becomes saturated. Finally in Fig. 7, the simulation for the Joule heating power that would be generated in a (10,10) CNT is plotted as a function of the temperature. From the figure it is fair to state that the temperature has more significant effect on the heat generated than the electric field force. As expected, as the temperature increases the scattering rates would increase and thus increasing the amount of heat that would be generated in the CNT. This is more significant at lower temperature, as a small increase in that range would have a significant effect on the Bose–Einstein distribution.

## V. CONCLUSIONS

A quantum mechanical model has been used to compute the Joule heating in CNT. The calculations are based on energy transfer during electron-phonon scattering and have been verified by comparison with experimental measurements for metallic SWCNTs. The Joule heating predicted

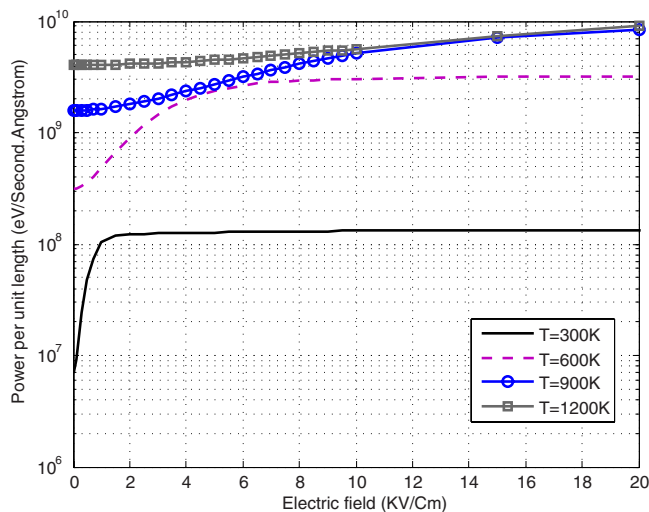


FIG. 7. (Color online) Heating power per unit length of CNT at different temperatures.

from the quantum mechanical model is compared with the classical ( $P=IV$ ) formula. The results show that the Joule heating in (10,10) CNT is two orders of magnitude less than what is predicted with ( $P=IV$ ), and thus making CNTs a good candidate to replace copper and aluminum as interconnect material for the next generation electronics. Analytical findings of this paper are supported qualitatively by experiments of Deshpande *et al.*<sup>26</sup>

## ACKNOWLEDGMENTS

The authors are thankful for Professor Peihong Zhang of the Department of Physics at the University at Buffalo for his helpful discussions. This project has been sponsored by NSF CMS Division under Grant No. CMS-0508854 and ONR Advanced Electrical Power Systems Division by Program Director Terry Ericson.

- <sup>1</sup>C. T. White, D. H. Robertson, and J. W. Mintmire, *Phys. Rev. B* **47**, 5485 (1993).
- <sup>2</sup>T. Ragab and C. Basaran, *Comput. Mater. Sci.* **46**, 1135 (2009).
- <sup>3</sup>E. Pop, D. A. Mann, K. E. Goodson, and H. Dai, *J. Appl. Phys.* **101**, 093710 (2007).
- <sup>4</sup>E. Pop, D. Mann, J. Cao, Q. Wang, K. Goodson, and H. Dai, *Phys. Rev. Lett.* **95**, 155505 (2005).
- <sup>5</sup>E. Pop, D. Mann, Q. Wang, K. Goodson, and H. Dai, *Nano Lett.* **6**, 96 (2006).
- <sup>6</sup>P. Vincent, S. T. Purcell, C. Journet, and V. T. Binh, *Phys. Rev. B* **66**, 075406 (2002).
- <sup>7</sup>M. A. Kuroda and J. P. Leburton, *Appl. Phys. Lett.* **89**, 103102 (2006).
- <sup>8</sup>A. P. Horsfield, D. R. Bowler, A. J. Fisher, T. N. Todorov, and M. J. Montgomery, *J. Phys.: Condens. Matter* **16**, 3609 (2004).
- <sup>9</sup>A. P. Horsfield, D. R. Bowler, A. J. Fisher, T. N. Todorov, and C. G. Sanchez, *J. Phys.: Condens. Matter* **16**, 8251 (2004).
- <sup>10</sup>A. P. Horsfield, D. R. Bowler, A. J. Fisher, T. N. Todorov, and C. G. Sanchez, *J. Phys.: Condens. Matter* **17**, 4793 (2005).
- <sup>11</sup>A. P. Horsfield, D. R. Bowler, H. Ness, C. G. Sanchez, T. N. Todorov, and A. J. Fisher, *Rep. Prog. Phys.* **69**, 1195 (2006).
- <sup>12</sup>A. P. Horsfield, M. Finnis, M. Foulkes, J. LePage, D. Mason, C. Race, A. P. Sutton, D. R. Bowler, A. J. Fisher, and R. Miranda, *Comput. Mater. Sci.* **44**, 16 (2008).
- <sup>13</sup>M. Lundstrom, *Fundamentals of Carrier Transport* (Cambridge University Press, Cambridge, 2000).
- <sup>14</sup>J. M. Ziman, *Principles of the Theory of Solids* (Cambridge University Press, London, 1972).
- <sup>15</sup>M. Steiner, M. Freitag, V. Perebeinos, J. C. Tsang, J. P. Small, M. Kinoshita, D. Yuan, J. Liu, and P. Avouris, *Nat. Nanotechnol.* **4**, 320 (2009).
- <sup>16</sup>L. Yang, M. P. Anantram, J. Han, and J. P. Lu, *Phys. Rev. B* **60**, 13874 (1999).
- <sup>17</sup>M. Verissimo-Alves, R. B. Capaz, B. Koiller, E. Artacho, and H. Chacham, *Phys. Rev. Lett.* **86**, 3372 (2001).
- <sup>18</sup>T. Hertel and G. Moos, *Phys. Rev. Lett.* **84**, 5002 (2000).
- <sup>19</sup>G. Pennington and N. Goldsman, *Phys. Rev. B* **68**, 045426 (2003).
- <sup>20</sup>R. Saito, G. Dresselhaus, and M. S. Dresselhaus, *Physical Properties of Carbon Nanotubes* (Imperial College Press, London, 1998).
- <sup>21</sup>G. Pennington, N. Goldsman, A. Akturk, and A. E. Wickenden, *Appl. Phys. Lett.* **90**, 062110 (2007).
- <sup>22</sup>A. Verma, M. Z. Kauser, and P. P. Ruden, *J. Appl. Phys.* **97**, 114319 (2005).
- <sup>23</sup>A. Akturk, G. Pennington, N. Goldsman, and A. Wickenden, *IEEE Trans. Nanotechnol.* **6**, 469 (2007).
- <sup>24</sup>A. Javey, J. Guo, M. Paulsson, Q. Wang, D. Mann, M. Lundstrom, and H. Dai, *Phys. Rev. Lett.* **92**, 106804 (2004).
- <sup>25</sup>J. Y. Park, S. Rosenblatt, Y. Yaish, V. Sazonova, H. Ustunel, S. Braig, T. A. Arias, P. W. Brouwer, and P. L. McEuen, *Nano Lett.* **4**, 517 (2004).
- <sup>26</sup>V. V. Deshpande, S. Hsieh, A. W. Bushmaker, M. Bockrath, and S. B. Cronin, *Phys. Rev. Lett.* **102**, 105501 (2009).